Cosmic ray observations with the Square Kilometre Array

S. Buitink,[a,b,*] **S. Bouma,**[c] **J. Bray,**[l] **A. Corstanje,**[a,b] **M. Desmet,**[a]
H. Falcke,[b,d,e] **B.M. Hare,**[e] **J.R. Hörandel,**[b,d,a] **T. Huege,**[f,a] **C. W. James,**[m]
N. Karastathis,[f] **P. Laub,**[c] **K. Mulrey,**[b,d] **A. Nelles,**[g,c] **O. Scholten,**[h,i]
R. Spencer,[l] **K. Terveer,**[c] **P. Turekova,**[e,h] **S. Thoudam,**[j] **G. Trinh,**[k] **S. ter Veen**[e]
and M. Waterson[n]

[a]*Vrije Universiteit Brussel, Astrophysical Institute, Pleinlaan 2, 1050 Brussels, Belgium*

[b]*Dept of Astrophysics/IMAPP, Radboud Univ. Nijmegen, P.O. Box 9010, 6500 GL Nijmegen, Netherlands*

[c]*Erlangen Centre for Astroparticle Physics, Friedrich-Alexander-University Erlangen-Nürnberg, 91058 Erlangen, Germany*

[d]*Nikhef, Science Park Amsterdam, 1098 XG Amsterdam, The Netherlands*

[e]*Netherlands Institute for Radio Astronomy (ASTRON), Postbus 2, 7990 AA Dwingeloo, The Netherlands*

[f]*Institut für Astroteilchenphysik, Karlsruhe Institute of Technology (KIT), P.O. Box 3640, 76021 Karlsruhe, Germany*

[g]*Deutsches Elektronen-Synchrotron DESY, Platanenallee 6, 15738 Zeuthen, Germany*

[h]*University of Groningen, Kapteyn Astronomical Institute, Groningen, 9747 AD, Netherlands*

[i]*Interuniversity Institute for High-Energy, Vrije Universiteit Brussel, Pleinlaan 2, 1050 Brussels, Belgium*

[j]*Department of Physics, Khalifa University, P.O. Box 127788, Abu Dhabi, United Arab Emirates*

[k]*Department of Physics, School of Education, Can Tho University Campus II, 3/2 Street, Ninh Kieu District, Can Tho City, Vietnam*

[l]*Dept. of Physics and Astronomy, The University of Manchester, UK*

[m]*Curtin University, International Centre for Radio Astronomy Research, Bentley, WA 6102, Australia*

[n]*SKA Observatory, Jodrell Bank, Lower Withington, Macclesfield, SK119FT, UK*

E-mail: stijn.buitink@vub.be

The low-frequency part of the SKA, to be built in Australia, will have an extremely high antenna density of roughly 60,000 antennas within one square kilometer, and is the perfect site for high-resolution studies of air showers. Individual showers will be observed with thousands of antennas simultaneously. The depth of shower maximum Xmax can be reconstructed with a resolution of 10 g/cm^2 using methods currently used by LOFAR and the Pierre Auger Observatory. However, the high-resolution SKA data allows the development of new methods that can reconstruct more features of the longitudinal development of air showers, such as the shower length or double-bump profiles. This allows new constraints on both the mass composition and hadronic shower physics. Here we discuss the status of the SKA cosmic-ray program and simulation studies of its capabilities.

---

*Speaker

1. The Square Kilometre Array

The Square Kilometre Array is currently under construction and will consist of two large arrays in Australia and South Africa. The Australian array covers the lowest frequency range (50 - 350 MHz) with log-periodic dipole antennas. A total of nearly 60 000 antennas will cover a circular area of approximately one square kilometer. The high antenna density and wide frequency band make the SKA a very interesting observatory for air showers. Operating the SKA as a cosmic-ray observatory will follow the same principle as LOFAR[1]: air shower detection constantly runs in the background while other astronomical observation are being performed. For this purpose, memory buffers are installed from which the cosmic-ray data is read out in case of a trigger. While triggering on the radio signal itself is not excluded as an option, the primary strategy is to use an array of particle detectors.

The right panel of Fig. 1 shows a map of the SKA-low site with antenna stations (consisting of 256 antennas each) as blue circles. An array of ~ 100 particle detectors (squares) will be installed at locations between these stations. Radio-noise is kept to a minimum by using silicon photomultipliers and RFoF cables for communication. Voltage control is needed for stable functioning under the strongly fluctuating temperatures in the desert. A prototype station of 8 units is currently under construction at the nearby Murchison Widefield Array [2] after earlier successful tests with a single station [3].

The size of the array limits cosmic-ray observations to an energy of $\sim 10^{18}$ eV. However, the SKA will reach lower energies than existing air shower radio experiments because of the possibility to use beam forming techniques with large groups of antennas. The large bandwidth also increases the sensitivity for antennas near the Cherenkov ring. The dense and homogeneous ground coverage ensures that this ring cannot be missed. Cosmic-ray mass composition studies will be possible down to at least $\sim 10^{16}$ eV. The energy range harbours the transition from a Galactic to extragalactic flux, which is still poorly constrained [4]. The SKA will make a unique contribution to our understanding of this energy range. However, the vast amount of data that are produced requires us to develop new approaches to air-shower reconstruction. Here we present progress in the exploration of the new capabilities that the SKA will offer.

2. Simulations

To study the performance of the SKA, Monte Carlo simulations were produced using COR-SIKA/CoREAS and an antenna model for the SKALA2 antenna design. A combination of instrumental and Galactic background noise was added. The left panel of Fig. 1 shows an example of a simulated shower. The radio footprint is covered by thousands of antennas simultaneously and its shape is directly visible. This is vastly different from event views of LOFAR or Auger[6], where fitted simulations are usually included to visualise the footprint. This alone will offer a unique test to radio simulation models.

As a first performance test, the standard LOFAR reconstruction techniques [7] were applied to the simulated events, yielding large improvements in the resolution: 50 cm in core position, 3% in energy, and 6–8 g/cm^2 in X_{max}. These values do not include systematic uncertainties related to the antenna model, atmosphere, and other factors [8].
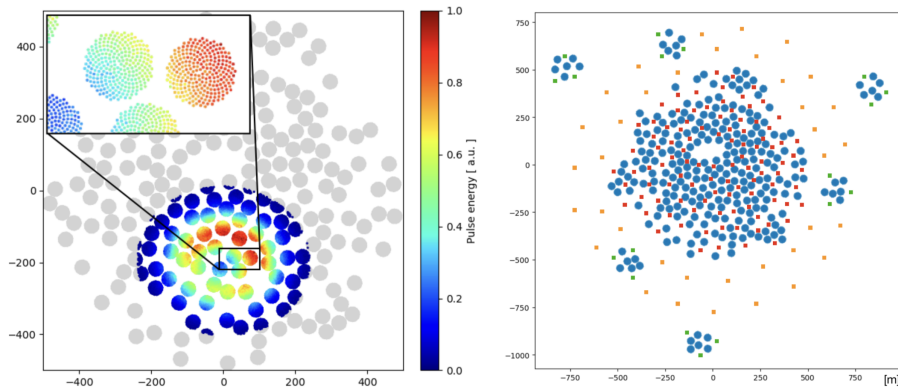
Figure 1: Left panel: simulated air shower observation for the SKA. The grey circles are antenna stations that each consist of 256 antennas, made visible by the zoom-in window. The color of the antennas indicated the fluence of the radio pulse. For grey antennas the signal-to-noise ratio is too low for detection. While the station locations are final, the exact positioning of antennas within a station is not yet fixed. **Right panel:** layout design for a particle detector array. The blue circles are antenna stations (including 6 satellite stations just outside the core). The squares indicate particle detector positions. The final design will be driven by available space between antenna stations and cable trench plans.

While these numbers are promising, air shower reconstruction with the SKA will require the development of techniques that are very different from LOFAR. First of all, the observed fluence in Fig. 1 is integrated over the full bandwidth, while the footprint shape is actually very dependent on the frequency, with a bean-like structure at low frequencies (e.g. LOFAR at 30-80 MHz) and a sharp ring at frequencies above $\sim$ 100 MHz. A better reconstruction quality can be achieved by properly taking the frequency-dependence into account. Moreover, the concept of fitting a limited set of simulated showers seems rather primitive for such detailed observations, as is illustrated dramatically by *double-bump* showers.

3. Double bumps

Double-bump showers occur when after the first collision of the cosmic-ray with an air molecule, one of the leading particles travels a large distance before interacting again. This results in a subshower that starts its development much later than the rest of the air shower. The longitudinal evolution of such a shower is very different from regular showers with a secondary bump deeper in the atmosphere (see top panel of Fig.2). Double-bump showers occur more frequently at lower energies, because the lower hadronic cross section increases the chance of having a very late second interaction. They are also more common for light mass primaries, because the fragments from the first interaction typically carry a larger fraction of the total energy, increasing the chance for the second bump to be detectable.

The direct observation of double-bump showers offers a new method to determine high-energy hadronic cross sections, provided the longitudinal evolution can be reconstructed. The bottom panel of Fig.2 shows a full simulation of a double-bump shower with instrumental and Galactic background noise included. Even by eye, the double structure is visible: the large ring corresponds
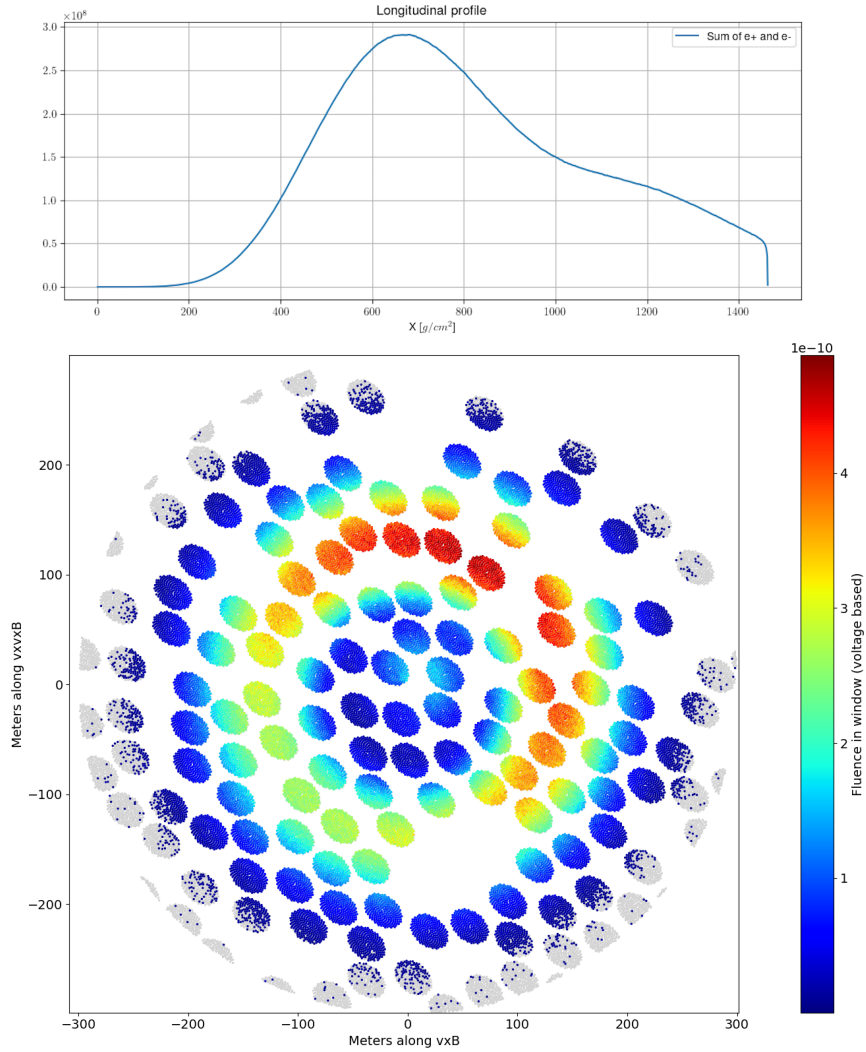
Figure 2: Top panel: Longitudinal evolution of simulated air shower with an energy of 5.6×10^{17} eV. The curve shows the sum of electrons and positrons in the shower, which has a secondary bump at $X \sim 1200$ g/cm^2. **Bottom panel:** Simulated radiation pattern including instrumental and Galactic background noise. The bright spot just off the center is caused by the secondary bump. Although it looks small in the picture, it still covers an area with hundreds of antennas.

to the primary maximum, while the secondary subshower produces the spot just off the center. While current reconstruction techniques cannot handle such an event, it is not unreasonable to expect that the atmospheric depth of both maxima can be reconstructed, as well as the fraction of energy that is contained in the secondary bump. Due to the high antenna density, even the inner spot still contains hundreds of data points.

The radio waveform itself also has unique characteristics for double-bump showers. The left panel of Fig. 3 shows a simulated pulse for an antenna located in the inner spot. It can be interpreted as the superposition of two pulses: the radio emission from the main shower does not have sharp features since the antenna is located far from the Cherenkov ring and only contains low frequencies.
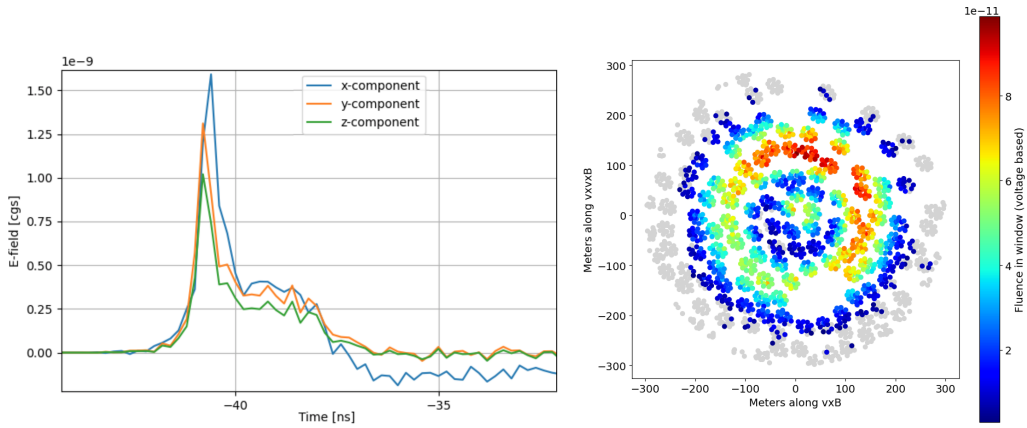
Figure 3: Left panel: Simulated waveform for an antenna inside the inner spot of a double bump shower (unfiltered). **Right panel:** Simulated radiation pattern including instrumental and Galactic background noise for a 7.4×10^{16} eV shower. Beam forming was applied to groups of 16 antennas.
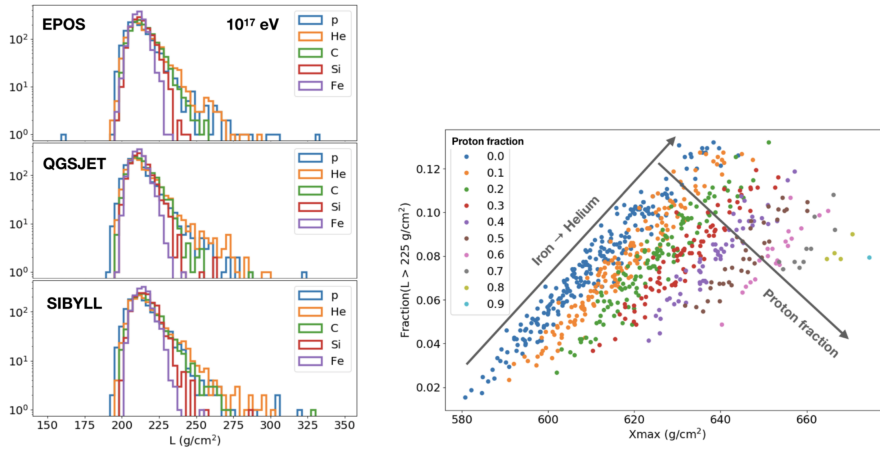
Figure 4: Left panel: L distributions for different elements based on CONEX simulations using QGSJETII-04, EPOS-LHC, and Sibyll 2.3d. **Right panel:** Average $X_{\max}$ and fraction of high-L showers for sets of showers containing different mixtures of five elements.

The Cherenkov ring of the second bump is much smaller on the ground and makes the sharp peak early in the waveform. There is also a time offset between the two contributions because the shower particles move faster than the radio waves in the atmosphere.

Since double-bumps occur more frequently at lower energies, it is essential to develop techniques that boost the signal-to-noise ratio (SNR). The right panel of Fig. 3 shows the footprint of a 7.4×10^{16} eV shower with some beam forming applied. The dots now represent groups of sixteen antennas. This boosts the SNR by a factor of four, while still maintaining a high number of data points for reconstruction. The double structure is still clearly visible.

4. Stretched showers

When the secondary subshower in a double bump profile moves closer to the main shower maximum it becomes increasingly harder to recognize it. In some cases the longitudinal profile can be fitted by a regular Gaisser-Hillas function but is still exceptionally stretched. This can be studied by using an alternative parametrization found in [9]:

$$N(X) = \exp\left(-\frac{X - X_{\max}}{RL}\right)\left(1 + \frac{R}{L}(X - X_{\max})\right)^{\frac{1}{R^2}},$$ (1)

where N is the number of particles in the shower, and X is the atmospheric depth in g/cm^2. The parameter L scales with the width of the profile and is a measure for the length of the shower, while R is a measure for the asymmetry in the profile shape before and after the shower maximum.

The left panel of Fig. 4 shows distributions of the L-parameter for various hadronic interaction models and elements. The same elements that have a larger probability of producing double bumps also have a larger tail in the distribution. Such *stretched showers* are more common than double bumps and a study of hadronic cross sections should include the two phenomena.

Moreover, stretched showers also provide important information on the mass composition. A very useful characteristic is that the fraction of stretched showers peaks at Helium. This allows for a better separation between proton and Helium when combining L and $X_{\max}$ measurements. This is illustrated in the right panel of Fig. 4. In this plot every point represents the average $X_{\max}$ and fraction of stretched showers for sets of 1500 showers of 10^{17} eV. The definition for a stretched shower is arbitrarily chosen here as exceeding 225 g/cm^2. Each of the sets contains a unique mixture of proton, Helium, Carbon, Silicon, and Iron, and is color-coded by its proton fraction. Together the sets form a triangular shape with sets containing specific proton fractions forming narrow bands. An improved p/He separation will help to identify the onset of the extragalactic component in the cosmic-ray flux, and to identify a possible Helium-rich secondary Galactic component due to supernova remnants of Wolf-Rayet stars [4].

5. Reconstruction challenges

Since the identification of stretched showers is valuable for both hadronic physics and astrophysics, we have started to develop new methods to use radio observations to constrain the longitudinal evolution of showers. It has already been shown in LOFAR data that changing L has a significant effect on the radio emission. The left panel of Fig. 5 shows the $X_{\max}$ reconstruction curve for a LOFAR event. Each dot is a simulated shower. In a plot of reduced χ^2 against the simulated $X_{\max}$-value, the lowest point of a fitted parabola is the reconstructed $X_{\max}$. When color-coding the point by their L-value it can be seen that this produces a shift in the curve. While L cannot be reconstructed with LOFAR, it is responsible for the scatter in data points, that lowers the $X_{\max}$ resolution.

The right panel of Fig. 5 shows a similar curve for SKA simulations. In this case all simulated showers have the same $X_{\max}$ but differ in R and L. It was found that a parabola fit can be done when plotting a linear combination R and L[8]. While this is a promising result, it is currently not
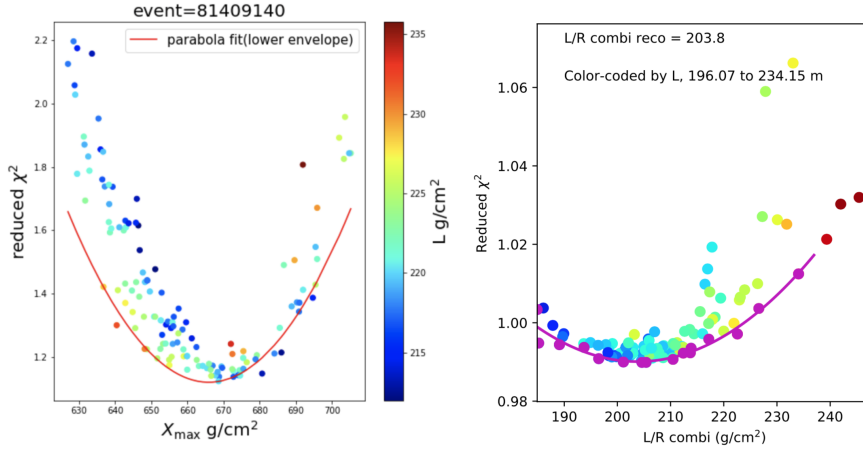
Figure 5: Left panel: X_{max} reconstruction curve for shower observed with LOFAR. The fit quality as a function of simulated X_{max} can be fitted by a parabola. The points are color-coded by simulated L demonstrating that the scatter around the parabola is in large part due to the longitudinal shape of the shower. **Right panel:** reconstruction curve for longitudinal shape of simulated SKA shower. The parameter on the x-axis is a linear combination of R and L, which can be accurately reconstructed if X_{max} is kept at a fixed (correct) value.

yet possible to simultaneously reconstruct X_{max} and L. The reason is that this would require and unreasonable amount of simulation.

This style of analysis relies on large sets of full CORSIKA/CoREAS simulations. A single simulation can take a few days of computation time on a single core. In order to do multi-parameter fits this approach has to be drastically changed. One possibility is to use a beam forming method to directly reconstruct the shape of the longitudinal evolution, as proposed in [10]. Alternatively, macroscopic simulation codes like MGMR3D can be used to do multiparameter fits[11].

A promising new technique is template synthesis. It is based on CORSIKA/CoREAS but stores the radio emission for different slices in the atmosphere and then uses scaling relations to produce radio pulses for arbitrary target longitudinal profiles. With this technique only one or a few simulations have to be run per observed shower. The method was already shown to reproduce full simulated waveforms with a bias of less than 2% for vertical showers [12] and is now generalized to arbitrary geometries [13].

6. Conclusion

The SKA will observe air showers in the energy regime between the knee and the ankle with ultrahigh precision. Radio footprint will be sampled by thousands of antennas simultaneously with a wide frequency band. This will not only allow high precision X_{max} observations, but also a more detailed reconstruction of the shower evolution. The observation of double bump profiles and stretched showers will lead to measurements of hadronic cross sections and additional mass composition sensitivity, in particular proton-Helium separation. This requires more advanced reconstruction and simulation techniques which are currently being developed.

References

[1] P. Schellart *et al.*,"Detecting cosmic rays with the LOFAR radio telescope", Astronomy & Astrophysics **560**, id.A98 (2013).

[2] A. Williamson *et al.*, "An Ultra-High Time Resolution Cosmic-Ray Detection Mode for the Murchison Widefield Array", J. of Astr. Instr., **10**, Issue 1, id. 2150003 (2021).

[3] J. Bray *et al.*,"The SKA particle array prototype: The first particle detector at the Murchison Radio-astronomy Observatory", NIMPA **973**, article id. 164168 (2020)

[4] S. Thoudam *et al.*, "Cosmic-ray energy spectrum and composition up to the ankle: the case for a second Galactic component", Astron. & Astrophys., **595** A33 (2016)

[5] A. Corstanje *et al.*, "Depth of shower maximum and mass composition of cosmic rays from 50 PeV to 2 EeV measured with the LOFAR radio telescope", Phys. Rev. D **103**, 102006 (2021).

[6] A. Abdul Halim *et al.* [Auger collaboration], "Demonstrating Agreement between Radio and Fluorescence Measurements of the Depth of Maximum of Extensive Air Showers at the Pierre Auger Observatory", Phys. Rev. Lett. **132**, 021001 (2024).

[7] S. Buitink *et al.*, "Method for high precision reconstruction of air shower $X_{\max}$ using twodimensional radio intensity profiles", Phys. Rev. D **90** 082003 (2014)

[8] A. Corstanje *et al.*, "Simulations of radio detection of cosmic rays with SKA-Low", **PoS(ICRC2023)500** (2023).

[9] S. Andringa, R. Conceição, and M. Pimenta, "Mass composition and cross-section from the shape of cosmic ray shower longitudinal profiles", *Astroparticle Physics* **34** (2011).

[10] H. Schoorlemmer and W. Carvalho Jr., "Radio interferometry applied to the observation of cosmic-ray induced extensive air showers", EPJC **81**, 12, 1120 (2021).

[11] P. Mitra *et al.*, "Reconstructing air shower parameters with MGMR3D", Phys. Rev. D, **108(8)**, 083041 (2023).

[12] M. Desmet *et al.*, "Proof of principle for template synthesis approach for the radio emission from vertical extensive air showers", Astroparticle Physics, **157**, 102923 (2024).

[13] M. Desmet *et al.*, "Applying template synthesis to the radio emission from air showers with generic geometries", **PoS(ARENA2024)046** (2024).